Photo-induced design of reflective metallized gold@polymer coatings with tuned architecture

Aleksandra Schejn, Murielle Ott, Marine Dabert, Loïc Vidal, Lavinia Balan

Materials and Design 160 (2018) 74–83

Contents lists available at ScienceDirect

Materials and Design

journal homepage: www.elsevier.com/locate/matdes

Photo-induced design of reflective metallized gold@polymer coatings with tuned architecture

Aleksandra Schejn [a], Murielle Ott [a], Marine Dabert [a,b], Loïc Vidal [a,b], Lavinia Balan [a,b,*]

[a] Université de Haute Alsace, Institut de Science des Matériaux de Mulhouse CNRS UMR 7361, F-68100 Mulhouse, France
[b] Université de Strasbourg, France

HIGHLIGHTS

- Photo-induced generation and structuration of gold nanoparticles in polymer matrix to design smart metallized surfaces.
- Innovative gold@polymer coatings with in situ control of the architecture via chemical and photonic parameters.
- An approach providing new solutions for large scale surface functionalization in view of industrial applications.

GRAPHICAL ABSTRACT

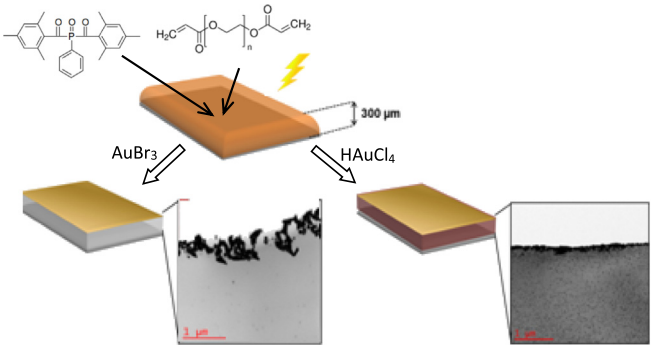

ARTICLE INFO

Article history:
Received 14 June 2018
Received in revised form 24 July 2018
Accepted 28 August 2018
Available online 30 August 2018

Keywords:
Metallized coating
Gold mirror
Photo-induced synthesis
Gold nanoparticles
Metal/polymer nanomaterials

ABSTRACT

This paper presents an efficient, eco-friendly, low cost and totally photo-induced approach to obtain new gold metallized coatings with highly reflective feature. Depending on gold precursor used and experimental conditions, the metal nanoparticles are distributed full depth or concentrated at the surface of the polymer matrix. The spatial organization and distribution of gold nanoparticles (AuNPs) is obtained through a perfect tuning of two concurrent processes, i.e. photo-polymerization of the binder and photo-reduction of the gold precursor to Au(0) nanoparticles, the balance of which is influenced depthwise, by internal filter effects associated to the absorption of gold particles or precursor. Two distinct classes of architectures were obtained. One of them was a bi-layered coating, i.e. a polymer rich sub-layer with a metal cover layer with a sharp delimitation between them; as for itself, the second type of metal@polymer coating exhibited a clear depthwise gradient of Au NPs concentration with a quasi-compact metal layer at the air surface. The mechanisms underlying these two types of architectures are discussed.
The metal@polymer coatings developed with this innovative approach are full of promise in many fields of application such as large scale functionalized surfaces, adaptive optical devices (plasmonic and mirror), flexible conductive surfaces and aesthetics.

1. Introduction

Metal nanoparticles (MNPs), such as silver, gold or platinum, have witnessed an outstanding interest in recent years due to their advantageous optical and physical properties that can be easily tuned by

* Corresponding author.
E-mail address: lavinia.balan@uha.fr (L. Balan).

https://doi.org/10.1016/j.matdes.2018.08.051

synthetic ways and also by assembling or well organizing these MNPs, leading to the numerous applications [1]. These can further be prominent for the fields such as photonics [2], information storage, electronic and optical detection systems [3–6], therapeutics [7,8], diagnostics, photovoltaics [9], catalysis [10,11].

To easily control the crystal morphology and thereafter, the physical and optical properties of MNPs, it is important to choose an appropriate synthetic method. Many synthetic routes are available for generating gold nanocrystals, such as the famous Turkevich's protocol (the citrate reduction method in water near boiling point) and Brust-Schriffrin's (effected in thiol-stable NPs) [12–14]. These chemical routes in principal, rely on the precipitation of gold nanoparticles (AuNPs) in aqueous solution from a dissolved gold precursor by reducers, e.g. sodium citrate, ascorbic acid, sodium boron hydride, or block copolymers [15–18]. Other procedures for AuNPs synthesis are mainly chemical, electrochemical, irradiation, sonochemical, solvothermal, photochemical and laser ablation using gold precursor either with or without presence of capping ligands [19–21].

Concerning the spatial control or assembling of the NPs, the most interesting are approaches leading to the formation of well-organized structures like films [22]. It was previously shown that the noble MNPs films provide novel and exceptional optical properties originating from increased density of localized surface plasmon resonance (LSPR). As an example, gold particles prepared as films gave much better performance, higher stability against corrosion, large electric conductivity and also possibility to control the surface chemistry to create well-defined molecular architectures [23]. These can be very useful in terms of plasmonic nanostructures used as optical antennas, nano-circuits, surface enhanced Raman spectroscopy (commonly known as SERS), biological and chemical sensors, conductive inks and photovoltaics [24,25]. Among various synthesis procedures for coating, a tremendous leadership has been given to electron beam lithography, nanoprint lithography, Langmuir-Blodgett, dip coating, electrochemical, liquid and vapor phase deposition [26–28]. However, these methods of fabrication present several drawbacks: they require sophisticated fabrication equipment, induce expensive cost or lack of mechanical strength [29]. To omit these inconveniences, hybrid materials based on gold and polymeric matrixes have recently drawn noticeable attention due to their synergetic effects [30]. Polymers fit well as suitable supports for MNPs dispersion [31]. The chemical composition of the polymer allows designing the scaffold's architecture of the hybrid and also influences the size and shape of the incorporated nanoparticles [32]. Polymer/MNPs assemblies are usually obtained using two main routes: ex-situ and in-situ approaches. In the ex-situ method, metal particles are synthesized beforehand and then, dispersed in the polymer. In the in-situ approach, the polymer matrix and NPs are created simultaneously [33,34]. However, synthetic paths for highly homogeneous polymer scaffolds are challenging as well as the control of self-organization of colloids onto substrates that normally requires either modification of the substrate or functionalization of the nanoparticles [35]. Among various strategies available to synthesize these complex systems, a promising one is based on the use of UV-light activation, which is able to induce the photo-polymerization of the organic matrix and at the same time, the photo-reduction of the metal precursor dispersed in the polymerizable formulation [36,37]. Moreover, it is an environmentally friendly approach that does not call upon toxic solvents or reactants; it is much faster and less energy-consuming.

In the previous works of our research group, a photochemical approach was applied to produce Au, Ag or Pd/polymer nanocomposites with controlled sizes and/or shapes, homogeneously distributed throughout the volume of the composite material [38].

The present paper is concerned with the photo-induced synthesis and spatial organization of nascent AuNPs in a polymerizable acrylate formulation with a view to promoting a novel approach to surface metallized coatings. Experimental studies aimed at getting a thorough insight into the mechanism of the UV-assisted spatial organization and assembling of the NPs and the tandem processes i.e. polymerization and reduction of Au^{3+} to Au(0), were carried out. The nanocoatings were optimized through a tailoring of the chemical and photonic parameters of the process. Thus, a new, efficient, fast and eco-friendly approach to control the in-depth assembling/organization of AuNPs in polymer materials is now available.

2. Materials and methods

2.1. Materials

Tetrachloroauric (III) acid (Hydrogen tetrachloroaurat(III)) ($HAuCl_4$) and gold(III) tribromide ($AuBr_3$), 99.9% were purchased from Sigma-Aldrich; polyethylene glycol (600) diacrylate (PEGDA oligomer) from Sartomer; bis(2,4,6-trimethylbenzoyl)-phenylphosphineoxide (Irgacure®819) was supplied by BASF and used without further purification.

2.2. Photo-induced synthesis

The polymer/gold films were prepared by simultaneous photo-induced reduction of gold ions (Au^{3+}) and polymerization of polyethylene glycol diacrylate monomer in the presence of a photoinitiating agent. Briefly, PEGDA was mixed with 0.5 wt% Irgacure 819 in an inactinic flask. In a separated vessel, gold bromide or tetrachloroauric (III) acid was dispersed in 100 μL of deionized water (per 3 g of formulation) by vigorous stirring during 1 h. Then, appropriate amounts of the two solutions were mixed so as to obtain a 1, 2 or 3% concentration of gold ions and stirred overnight. The resulting formulation was homogeneously applied at the surface of a glass slide with an automatic device for film deposition (byko-drive Auto Applicator). Hamamatsu Lightningcure LC8 (Hg-Xe L8252) was used to activate the photochemical reactions. The light intensity delivered by the light source in the 300–450 nm window. In a typical arrangement, the sample was placed horizontally under the UV–Vis lamp operating at 450 or 770 mW/cm^2 and the reaction was carried out for 40 min. Then, the sample was characterized using UV–Visible spectroscopy, transmission electron microscopy (TEM), X-ray diffraction and real-time FT-IR analysis.

2.3. Instruments

UV–vis spectra in transmission mode were recorded with an Evolution 220 Thermo Scientific spectrophotometer. The wavelength resolution was 1 nm. Samples deposited on the glass slides were measured using a slide holder that ensures reproducible positioning. The particles morphology was confirmed by TEM imaging technique. The measurements were performed with a Philips CM20 instrument with LaB6 cathode at 200 kV. Crystallographic data were collected with a Philips X'Pert MPD diffractometer equiped with a Cu Kα radiation $\lambda = 0.1546$ nm running at 40 kV and 40 mA. The polymerization kinetics were analyzed by using a RT-FTIR Avatar spectrophotometer on samples deposited on CaF2 pellet irradiated with a Hamamatsu Lightningcure source LC8 (Hg-Xe L8252) delivering 74 mW/cm^2. During the irradiation time the temperature was constantly 35.6 °C.

3. Results

The photosensitive formulation used in this work consisted of a gold precursor, a diacrylate monomer and a photogenerator of free radicals (bis-(2,4,6-trimethylbenzoyl)-phenylphosphineoxide). Gold bromide ($AuBr_3$) and hydrogen tetrachloroaurate(III) hydrate ($HAuCl_4.xH_2O$) were used as the gold source.

In order to obtain well-defined and homogeneous films, the reactive formulations were deposited on a glass slide with a constant thickness of 300 μm by using an automatic applicator device. The samples were exposed horizontally to the UV lighting device to generate the metal-

polymer nanocomposite coating via a complex sequence of photo-induced reactions.

The influence of both gold precursor concentration (from 0 to 3 wt%) and fluency of the UV-light source (450 and 770 mW/cm^2) was investigated.

The photosensible formulations containing $AuBr_3$ at concentrations ranging from 0 to 3 wt%, were characterized by UV–Vis spectroscopy; the results are shown in Fig. 1 (since the samples with 2 and 3% Au behaved similarly, only one spectrum was reported for clarity of the graph). With both intensities (450 and 770 mW/cm^2) and after 40 min UV-exposure, two surface plasmon resonance peaks related to gold nanoparticles developed at 557 and 960 nm, and 553 and 960 nm, respectively.

The time evolution of UV–Vis spectra of the samples synthesized with both gold precursors ($AuBr_3$ and $HAuCl_4$) is reported in Fig. 2. The digital photographs of the samples were taken at different exposure time to show also the progress of the reaction during the illumination (Fig. 2).

The changes in UV–Vis spectra are related to the formation of gold nanoparticles and modification of their size and shape. These changes are consistent with what is observed on the photographs of the samples taken at increasing time exposures (see photographs Fig. 2). The formulation containing $HAuCl_4$, initially pale yellow, turned very quickly to intense purple upon irradiation, which reveals the formation of a high concentration of gold NPs. At longer exposures, a coalescence of the particles took place in the upper part of the layer, which led finally to the formation of a compact continuous nanolayer of gold.

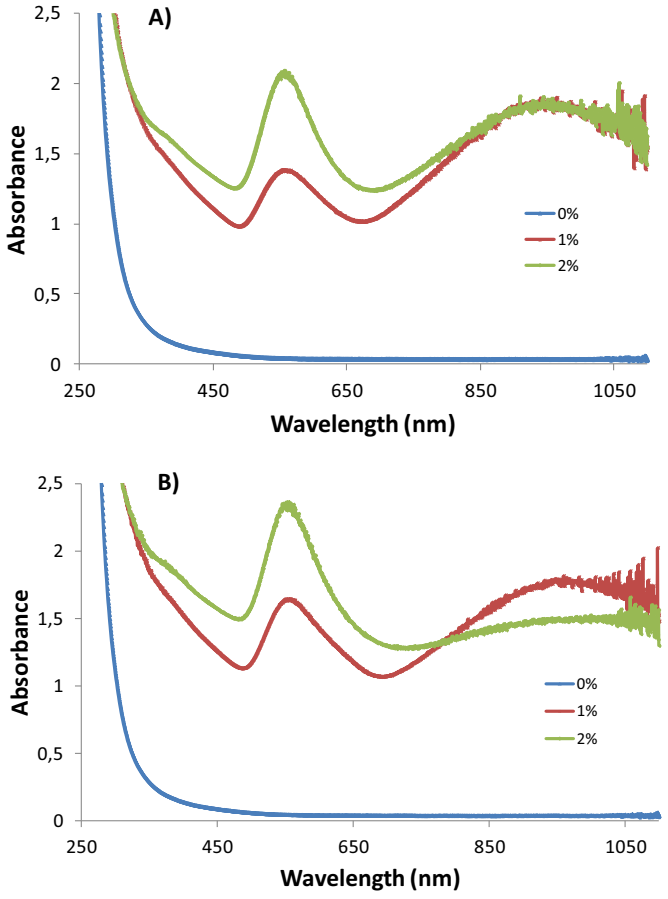

Fig. 1. UV–Vis spectra of the nanomaterial coating obtained by playing with the concentration of $AuBr_3$ gold precursor and light intensity: A) 450 and B) 770 mW/cm^2, exposure time 40 min, film thickness 300 μm.

A similar behavior was observed with the formulation containing $AuBr_3$ at the beginning. The orange brown colour of gold bromide precursor faded after 1 min exposure and turned to slightly purple, thus revealing the formation of gold seeds. By continuing the irradiation, the nucleation/coalescence process developed until a golden layer was formed (see Fig. 2).

In both cases ($AuBr_3$ and $HAuCl_4$), after 10 min, the samples exhibited a clearly golden shiny metallic aspect with a high reflectivity.

The results of TEM characterizations are shown in Fig. 3. The samples were prepared using cryogenic microtome to slice down the nanomaterial on the cross section of the layers. The micrographs confirm the presence of gold nanoparticles in the polymer matrix and also reveal a spatial organization of the superficial-gold nanostructure. The particles appeared mostly round-shaped and during the first 20 min of the reaction, irregular polygonal shapes and dimers were also observed. In the case of $AuBr_3$, gold nanoparticles concentrate at the top surface of the sample, while in contrast, they are distributed all over the thickness of the sample with a marked top-to-bottom gradient of concentration when $HAuCl_4$ is used as the gold precursor. Upon increasing the exposure, bigger particles were created by association of smaller ones to form either anisotropic or elongated branched structures with both precursors (see Fig. 3A and B for a 40 min exposure). This coalescence process was especially visible near the top surface. The development of a second plasmon band in the far red (ca 960 nm for $AuBr_3$ and 760 nm for $HAuCl_4$ (Fig. 2)) gives support to this analysis.

The selected area electron diffraction pattern (SAED) analysis (Fig. S1) confirmed the polycrystalline character of the samples. The recorded patterns present several Bragg reflections originating from individual crystallines forming together multi-spot circles, each of them corresponding to one of the characteristic planes (111), (200), (220), (311) and (222) of Au(0).

X-ray diffraction analysis was used to confirm the formation of Au (0) particles and identify their crystalline structure within the polymer matrix. As shown in Fig. 4, the peaks indexes at 38°, 44°, 64°, 77° and 81° indicate the presence of (111), (200), (220), (311) and (222) planes of Au(0) respectively (JCPDS card no. 04-0784). No additional peaks that could belong to undesired impurities or by-products were detected in the samples. The higher intensity in the (111) signal in the XRD patterns suggests a prevalence of fcc structure in both systems ($AuBr_3$ and $HAuCl_4$).

The PEGDA polymer was chosen according to its outstanding properties. It provides transparent, clear, non-toxic, flexible and free-radically curable films. PEGDA polymers can be easily polymerized by radical initiation under either ultraviolet irradiation or thermal activation [39,40]. The polymerization process includes several steps: absorption of the light by the photoinitiator, formation of 2,4,6-trimethylbenzoyl and phenylphosphonyl radicals that provide activation of unsaturated bond of PEGDA and propagation of the crosslinking polymerization and finally, termination of the polymerization. In the present study, a real-time FT-IR analysis was used to follow up the decrease of the absorption associated to the C═C stretching vibration at 1636 cm^{-1} during the irradiation. The degree of conversion was recorded with a UV–Vis intensity of 74 mW/cm^2 and a 25 min exposure. The results are reported in Fig. 5. Two types of measurements were carried out, with and without gold, and compared. In a first approach, the influence of the gold-precursors and their concentrations on the polymerization process was examined. For both precursors used in this study, the conversion curves revealed a decrease of the polymerization rate with increasing the concentration of gold precursor. The polymerization started all the slower as the gold precursor content is higher but at the end of the exposure, the same plateau is reached i.e. after 20 min, a. 80–90% conversion of the ethylenic double bonds. Interestingly, no change was observed in the regions of 1725 and 1110 cm^{-1}, which correspond to the C═O and C—O asymmetric stretching vibrations of the C—O—C groups. As a consequence, it can be concluded that the light used for this experiment does not affect the structure of the

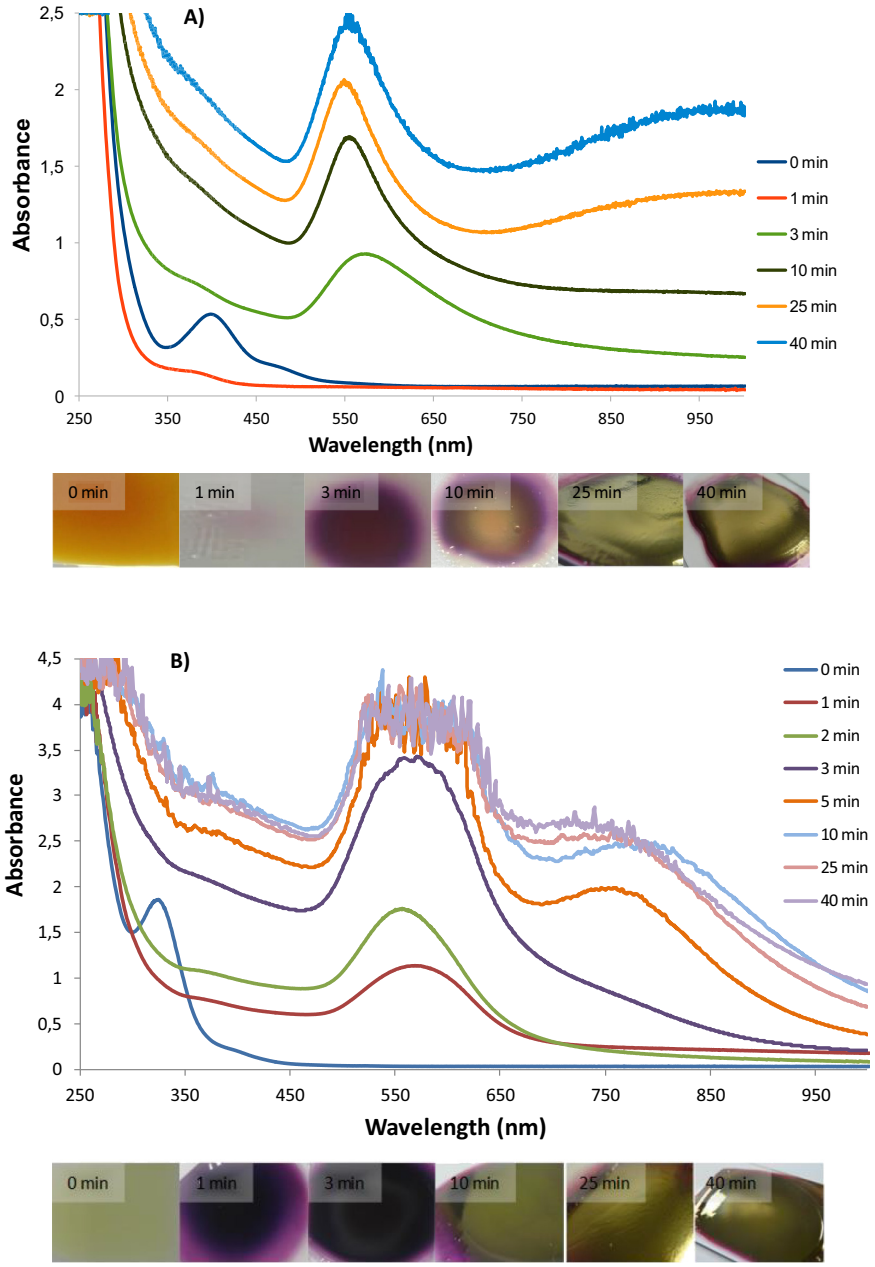

Fig. 2. UV–Vis spectra and corresponding images of the composite coatings obtained with increasing exposure time: A) $AuBr_3$ and B) $HAuCl_4$ precursors; concentration 2 wt%, light intensity 450 mW/cm^2 and film thickness 300 μm.

PEGDA polymer in itself but only the conversion rate of C═C to C—C bonds.

In order to confirm that the reaction mechanism of gold@polymer nanoassemblies formation involved a photoinduced and not a thermal process, the same experiment was carried out in the absence of actinic light and at increasing temperatures to check how the formulation behaved under such conditions. No change in the colour was observed up to 100 °C. The film started to harden and turned very slightly brownish-violet from 120 to 180 °C, indicating that traces of gold seeds are generated in this temperature range. Then, around 265 °C, the samples underwent carbonization.

Fig. 6 shows the metal@polymer coatings with gold and their highly reflective/mirror properties. Interestingly, by scraping only the top metal surface with a scalpel, it was also possible to make evident the difference in the mechanism of action between the two precursors in terms of structuration of AuNPs in the polymer matrix:

i) in the case of $AuBr_3$ (Fig. 6A), in its initial state, the sample exhibited a gold and shiny metallized aspect and after scratching the top golden surface, the composite layer became quasi translucid, thus confirming the presence of very small quantity of NPs in the depth of the material (few nanoparticles can still be presented) (Fig. 6Ab).
ii) in the case of $HAuCl_4$, the scratched sample appeared dark violet without any transparency, which confirms the presence of an important concentration of AuNPs in the core of the composite layer (Fig. 6B).

The gold@polymer coatings exhibit interesting reflective properties which were quantitatively characterized through their reflectance spectra (Fig. 7). The sample obtained from $AuBr_3$ showed a reflectance exceeding 90% in the red, very close to that of optically polished bulk gold [41]. In the case of $HAuCl_4$, the reflectance is around 60%. In both cases, the reflectance decreases dramatically below 500 nm (Fig. 7).

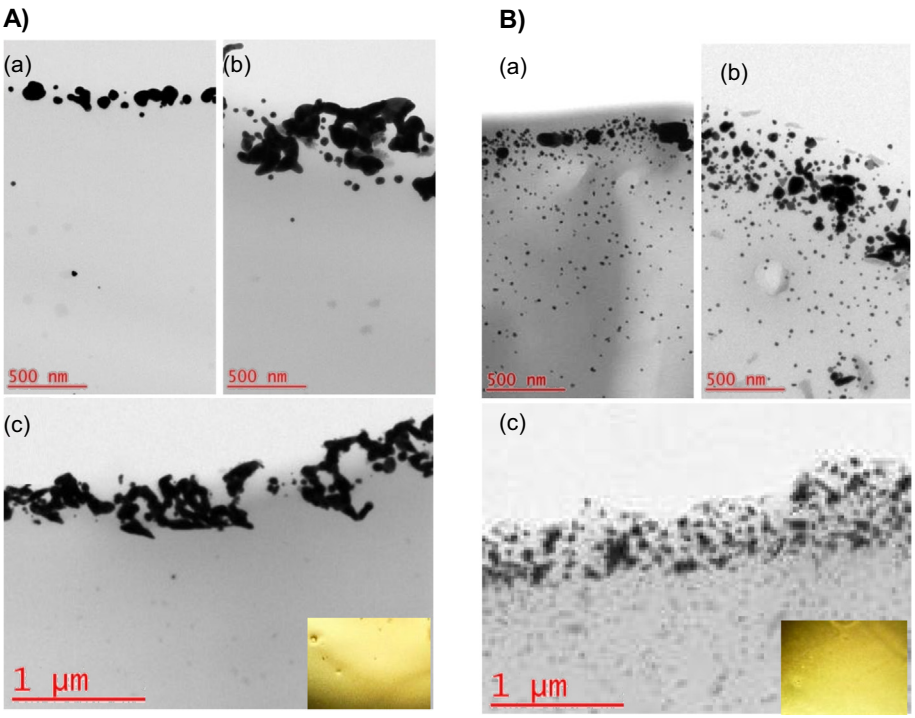

Fig. 3. TEM micrographs (cross sections from the top-air side to the bottom of the coatings) of the synthesized coatings: A) with $AuBr_3$ and B) with $HAuCl_4$; (a) after 20 min, (b) & (c) 40 min UV-exposure, thumbnail and overview, respectively. Light intensity 450 mW/cm^2 and film thickness 300 μm.

Moreover, the absence of the LSPR peak confirmed that particles are in contact with their neighbors and form a quasi-continuous gold layer.

The SEM image (Fig. S2), shows a fairly regular surface topography of the layer, with gold nanoparticles uniformly distributed and tightly arranged. These observations are quite consistent with the macroscopic optical appearance of the layers. This confirms the good surface quality of this nanomaterial.

4. Discussion

It is a well-known fact that both photopolymerization and photo-reduction of metal cations involve a radical arising from homolytic photocleavage of the C—P bond of Irgacure 819, which generates 2,4,6-trimethylbenzoyl and phenylphosphonyl radicals. The general mechanism of the photoinduced synthesis of MNPs in a photopolymerizable formulation to generate nanocomposite materials where NPs are homogenously dispersed in a polymer binder, was thoroughly described in a previous work [38a]. In the present work, advantage was taken of specificities of the gold precursors used to induce two interesting and unprecedented inhomogeneous distribution profiles of the MNPs in the polymer layer. Moreover, the corresponding materials were obtained through a one-step photochemically activated process.

In this context, the discussion focuses on the reasons that are behind the in-depth inhomogeneity of the metal@polymer nanomaterials and the respective influence of photonic and chemical parameters on the creation of such spatial AuNPs organizations.

In its initial state, the photosensitive formulation containing $AuBr_3$ with orange-brown colored. It contained mostly the $[AuBr_3(OH)]^-$ complex, which exhibited a main band centered at 400 nm and a

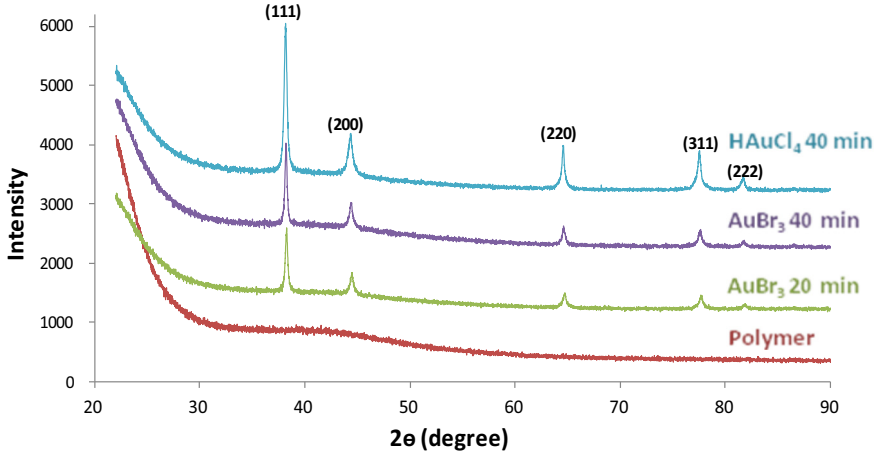

Fig. 4. XRD patterns of a 300 μm composite coating and the reference polymer matrix; light intensity 450 mW/cm^2, time exposures: 20 min and 40 min.

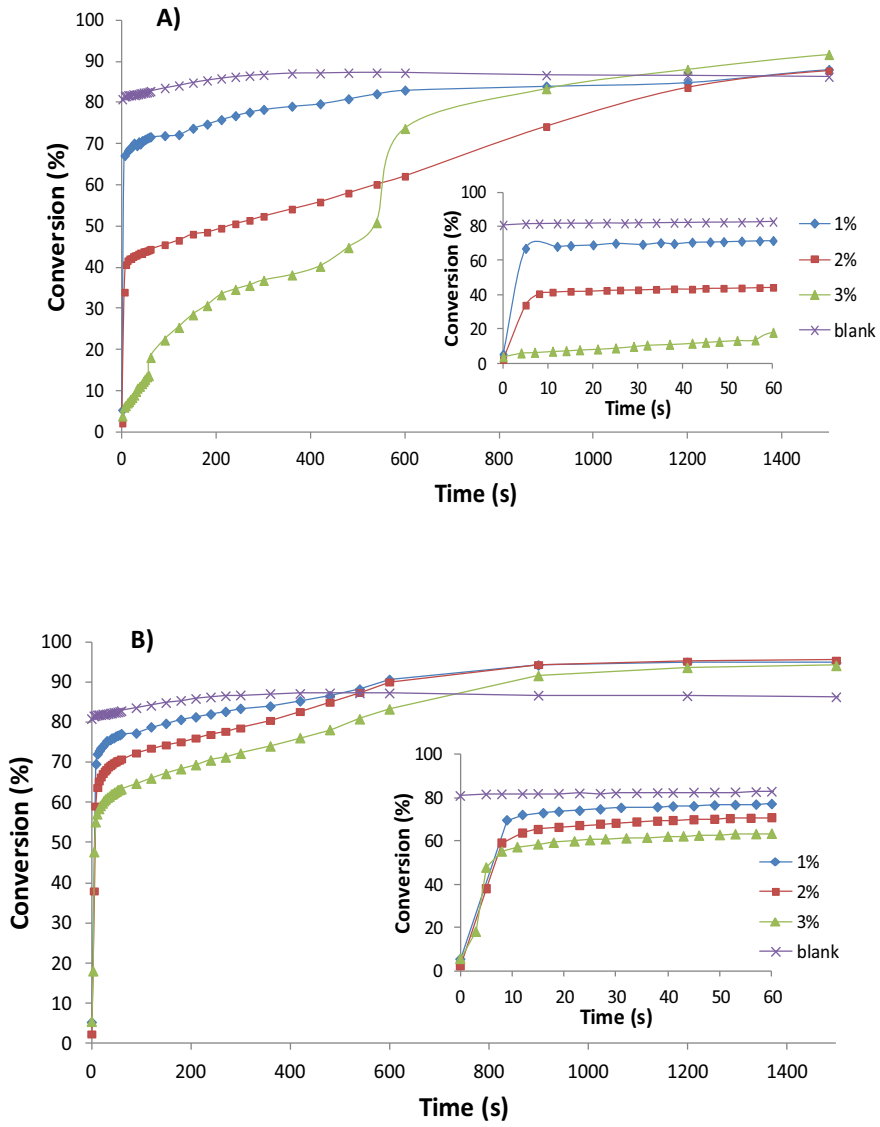

Fig. 5. Real-time FT-IR conversion curves as a function of the irradiation time for blank PEGDA and PEGDA containing 1, 2 and 3 wt% of A) $AuBr_3$ and B) $HAuCl_4$ gold precursor. Light intensity: 74 mW/cm^2.

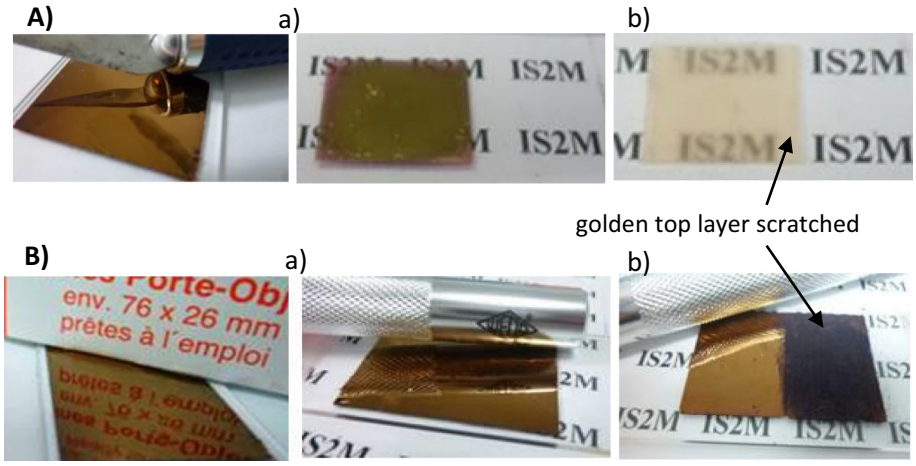

Fig. 6. Digital photos of the gold@polymer mirror coatings prepared with A) $AuBr_3$ and B) $HAuCl_4$, before and after scratching the golden superficial layer.

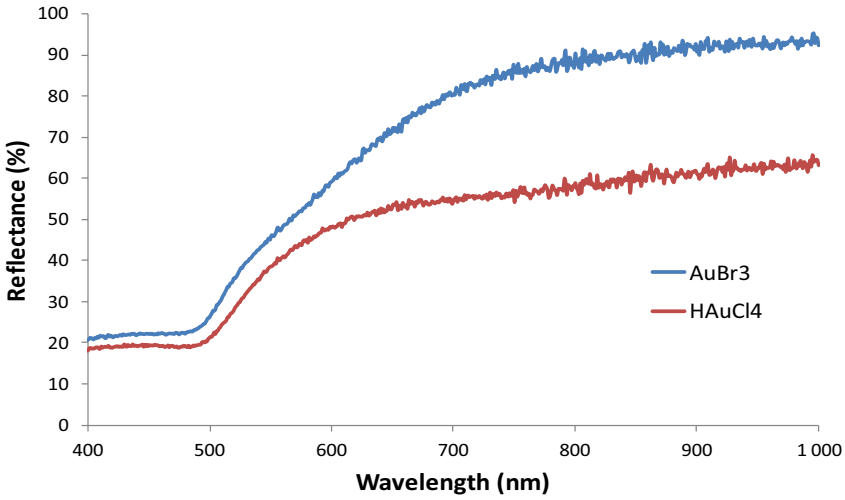

Fig. 7. Reflectance spectrum of the gold@polymer coating with $AuBr_3$ and $HAuCl_4$ precursors.

shoulder in the blue, spreading up to 550 nm (see blue spectra Fig. 8A). These observations are in good agreement with the spectroscopic study of the tetrahydroxo-bromo complexes of gold in aqueous solution published by Al Usher et al. [42]

During the first 20 s of the photolysis, the solution bleached and turned colorless. This observation is interpreted as the first step of the photo-reduction that converts Au(III) to Au(I) (see red spectra Fig. 8A). The corresponding $Au(I)Br_2^-$ complex is known to absorb deeper in the UV with a maximum around 256 nm in polar solvents [43]. Due to the own absorption of the pyrex-glass slide, this band is not visible on Fig. 8A. Since the absorption of the hydroxo-tribromo complex of Au(III) coincides with the active range of Irgacure 819, it

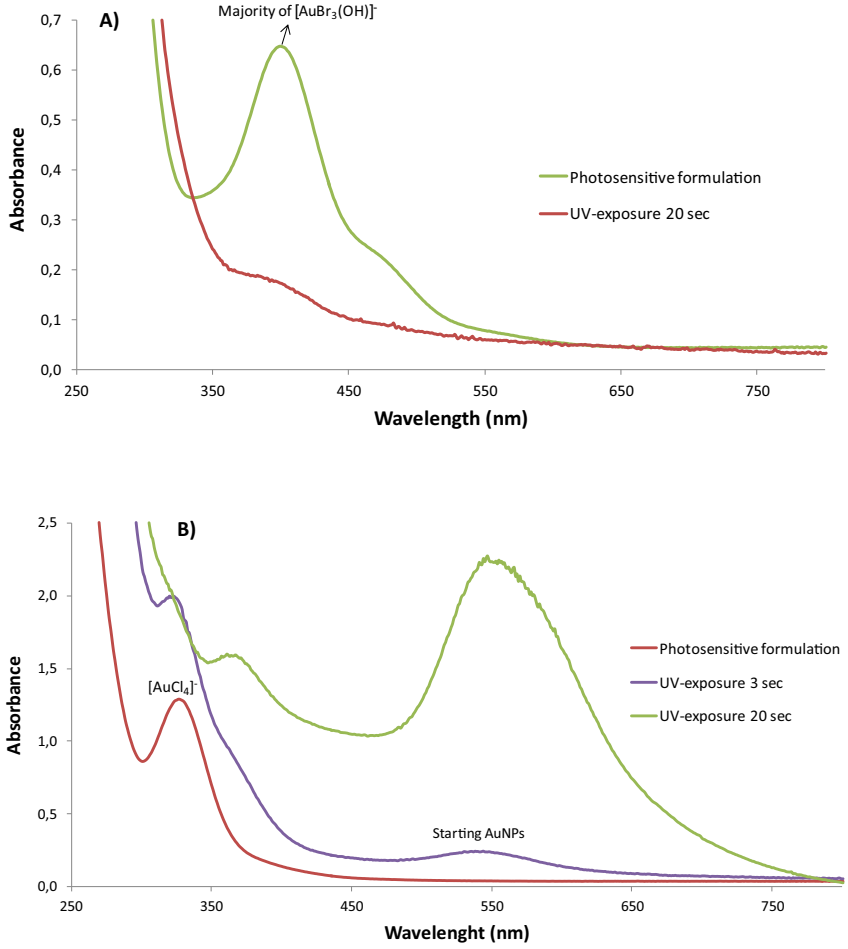

Fig. 8. A) UV–Vis spectra of Au(III) complexes of A) $AuBr_3$ and B) $HAuCl_4$: initial formulation and first moments of the photolysis.

induces an internal filter effect, which results in a very slow rate of conversion of the monomers during this first stage of the process (Fig. 5A). Clearly, a front of bleaching has to propagate from the top to the bottom of the formulation before the polymerization reaches its stationary rate. In another respect, during the first moments of the process, the internal filter effect due to the absorption of bromo-hydroxo complexes confines the photoreduction of Au(III) to Au(I) to the very first nanometers of the reactive layer. As a consequence, a concentration gradient of Au(III) species is created, which induces a diffusion of these species from the core to the top of the layer to equalize their chemical potential. The result is an accumulation of Au(I) complexes near the surface of the sample. This phenomenon is all the more pronounced as the concentration of the gold precursor is high. After a 3 min exposure, a new band developed at 575 nm, which is assigned to the typical LSPR of gold nanoparticles (see Fig. 2). This behavior is accounted for by the reduction of Au(I) to Au(0). As the irradiation proceeds, the LSPR band exhibited a slight blue-shift thus indicating an increase of the refractive index of the polymer matrix (1.47) and a decrease of the average interparticle distance [44]. Upon longer exposure (>25 min), a second multiple broad LSPR band located around 960 nm developed. It is assigned to a second population of gold particles with bigger sizes resulting from the aggregation of smaller ones and some elongated shapes due to the coalescence of nanoparticle twin, dimers (see TEM, images Fig. 3A), the LSPR of which contributes to this second far-red absorption band [45,46].

Since the first step of the process induced an accumulation of Au (I) near the surface of the layer, a much higher concentration of nascent gold particles is produced by the second step of the reduction in this part of the sample. As the irradiation proceeds, due to the coalescence between nanoparticles, a quasi-compact and continuous metal layer is formed. The final result is a bi-layered architecture with a very thin gold metal top layer and an underlying polymer layer containing only a few scattered gold NPs (see cross section TEM of the sample Fig. 3A). In the experimental conditions prevailing, the thickness of the metal layer is around 350–400 nm with an overall gold@polymer coating thickness of ca. 300 μm (Fig. 6).

As regards $HAuCl_4$, the second gold precursor used in this study, the main difference with $AuBr_3$ lies in the region of absorption. $[AuCl_4]^-$ absorbs deeper in the UV (between 300 and 370 nm), outside the region of absorption of the generator of free radicals. Consequently, $HAuCl_4$ does not induce any internal filter effect at this stage. Since the very beginning of the irradiation, a new band centered at 530 nm emerges, which reveals the presence of small Au(0) particles around 10–20 nm (see spectra at 3 s exposure - Fig. 8B). It must be concluded that the photo-reduction process starts from the first moments of the photolysis and that the reaction rate is much faster than in the case of $AuBr_3$ (where the reaction starts after 1 min exposure, only).

As the reaction proceeds beyond 3 mn exposure, both the intensity of the plasmon band and the concentration of Au(0) nanoparticles increase steadily. The development of a second LSPR band centered at 760 nm reveals an aggregation process of the particles to bigger polygonal and elongated crystallites see TEM images (Fig. 3B). By comparison, this behavior was observed in the case of $AuBr_3$ only after 25 min irradiation and much further at ca 960 nm (see Fig. 2A and B).

Moreover, the distribution of gold nanoparticles with a more or less pronounced in-depth gradient of concentration must be related to the fact that the absorption spectrum of the gold precursor does not induce significant internal filter effect on the light activation of the free radical generator. Because of this, the in-depth profile of the particles concentration is governed by the progressive darkening associated to the presence of bigger metal particles that attenuate the penetration of actinic photons through reflection and diffusion. The same behavior was already observed in our recent works devoted to the synthesis of silver NPs [47].

Incidentally, when $KAuCl_4$ was substituted for $HAuCl_4$ as the gold precursor, it is worth of notice that the same behavior and structuration of the NPs in the polymer matrix was observed.

In both cases, the TEM micrographs confirm the specific structuration of the nanoparticles function of the precursors used. With the increased exposure time, the coalescence of the AuNPs on the top of the coating increased until a quasi-compact gold layer formed. (see TEM micrographs and digital pictures of the samples). The TEM images recorded with both samples revealed that the population of the biggest particles is localized at the top surface of the films.

Moreover, these observations are also in line with the RT-FTIR kinetic study of the C═C conversion as a function of the Au concentration. Since the polymerization photoinitiation and gold cations photoreduction are concurrent processes, increasing the concentration of gold cations favors the reduction process at the expense of the polymerization in both cases. With $AuBr_3$ the time profile of the polymerization rate shows a very slow conversion at the beginning of the process, which must be assigned to the detrimental internal filter effect induced by the gold precursor also (see Fig. 5A). In the case of $HAuCl_4$, the polymerization and formation of gold NPs happened quasi simultaneously in the whole depth of the sample under the only control of the in-depth light absorption by the radical generator (see Fig. 5B).

As regards the plasmon resonance of the gold nanoparticles formed with both precursors, upon increasing the exposure time, clear differences were observed in the coalescence and agglomeration process. At the same time, a different depthwise organization in the polymer matrix was observed, especially on the top gold layer of the nanoassembly. At the beginning of the UV exposure, the nanoparticles were mostly round shaped in both cases; they rapidly started to fuse together to form more complex architectures especially near the top surface (see Fig. 3). This is consistent with the appearance of the second band on the far red side of the absorption spectra for both precursors (Fig. 2). To explain, the irradiation energy continuously applied during the process increased the surface energy of the already synthesized particles, thus making them tending to reduce it by coalescence and agglomerations into bigger forms. As a result, this energy is responsible for dissolution of unstable phases such as small particles or metastable polymorphs and leading to much more stable phases with diminished energy surface [48]. In the samples obtained with $AuBr_3$ as the gold precursor, after 20 min exposure, twin, dimeric particles that started to interconnect with big gaps between such agglomerates located at the surface were observed. After 40 min, the particles tended to form very randomly branches resulting from the extensive overgrowth from templates previously created (see Fig. 3A). With the sample synthesized with $HAuCl_4$, after 20 min, two populations of particles that were randomly dispersed within the polymer matrix were visible: a smaller one with a diameter of about 10–20 nm and a bigger one with size of approximately 45 nm for dimers and 100 nm for agglomerates. After 40 min, a tendency to create branched but mostly twin-like structures at the top surface was also observed. As shown previously, the development of the second band in the UV–Vis spectra can be understood by considering the morphology or arrangement of nanoparticles formed in the polymer nanoassembly by the two modes of oscillations, i.e. transverse mode (along short axis) and longitudinal mode (along long axis) [45,46]. The second band can also originate from the decrease in the interparticle distance and formation of particles welds as given with the effective medium theory of Maxwell Garnett. This can of multi-shaped samples have already been reported in the thermal synthesis of Au/polymer hybrid structure, as example by Porel [49]. Their work revealed that the regularity of shapes in AuNPs formation within PVA polymer by thermal treatment can be adjusted with increasing the concentration, decreasing temperature or increasing heating time. They also indicated the fact that in situ generation of nanocrystals in polymer films using the matrix as the only reagent results in free-standing films with embedded particles of different shapes. It was also pronounced by the group of Chao [50]. This polycrystallinity of gold particles originates for the bimodal growth mechanism of Ostwald, ripening and coalescence, simultaneously. Another work of Harada showed that the photoreduction process of $[AuCl_4]^-$ precursors in

poly(*N*-vinyl-2-pyrrolidone) resulted from the nucleation and subsequent aggregative growth of the colloidal gold nanoparticles [51]. As suggested previously, to explain the formation of broad second band at the UV–Vis spectra, most of the groups applied the Maxwell Garnett effective medium theory that relies on the influence of interparticle distance on the optical characterization of the system [52–54].

The metal and mirror aspects on the top layer are clearly related to the dense amount of gold particles accumulating at the top surface of the nanomaterial coating during the irradiation process. The gold nanoparticles started to aggregate and form bigger agglomerates and then the surface became more irregular and rough (see TEM and SEM images). When the incident light strikes this surface, it is reflected at first specularly and then in all directions, thus accounting for the mirror aspect of the samples [55]. Longer exposures induce a degradation of the surface flatness that goes along with an accentuation of its diffusive character (Figs. 2 and 6).

The observed phenomena of gold mirror surface grounds the knowledge on nanoassemblies architecture dependent optical characteristics. El-Sayed et al. indicated that single nanoparticles generate moderate signal, while aggregations increased the scattering Raman signal [56]. As was also shown by Siegel et al., properties of metal layers are affected by electron scattering on phonons, imperfections and at the layer boundary that is also responsible for reduction of the electric conductivity of thin layers [57]. The second harmonic generation of light in reflection from metal by the incident light was also reported by Zayats [58]. They explained the roughness-induced excitation of a surface plasmon polariton (SPP) by the incident light, which in turn enhances the nonlinear source term in the Maxwell equations responsible for the reflected light at twice the frequency of the incident light.

The metallized gold layer created at the coating surface, it was also in relation to Leosson and Kang works [59]. They showed random organization of assemblies with many voids, surface defects and inhomogeneities. This roughness significantly enhances the SPPs to Bragg scatter and being decayed in a non-radiative way, i.e. in a form of light. Localized surface plasmons LSPs can be excited and can decay in SPPs. Kang observed that for nanogap-rich gold nanoislands with increased diameter of this peculiar morphology of nanoparticles assemblies the increase in extinction intensity with following red-shift of the plasmon resonance wavelength that was associated also with increase in number of plasmonic hotspots and decrease in gap spacing between islands through coalescence. Presented literature confirms influence of the gold nanoparticles formation on the presence of visual gold mirror aspect as outcomes of our work.

5. Conclusion

In conclusion, we developed an all photo-induced and advantageous organization of gold nanoparticles in the polymer matrix. In our hands, we managed to control the polymerization rate and the photoreduction of nanoparticles rate by using different internal filters to obtain two architectures of gold@polymer coatings. The approach developed in the present work allows obtaining innovative metallized surfaces with high reflective and mirror aspect and the corresponding nanomaterials exhibit attractive properties. Moreover, the photochemical approach used to fabricate these materials brings new solutions for industrial applications with high environmental and economical impact. The ease of implementation, eco-friendly character (without solvents and toxic reactives) and low operating cost are decisive advantages in view of future applications of the developed nanomaterials in areas such as optics, decoration or catalysis.

Moreover, conclusive preliminary tests conducted on substrates other than glass slides like woven or non-woven fabrics, should open an avenue for flourishing innovative applications.

Author contributions

LB conceived the idea. MO, AS, MD and LB performed the experimental synthesis, characterization and properties of the gold@polymer nanomaterials. LV performed the TEM images. LB coordinated the manuscript preparation. All authors give the approval for the final version of the manuscript.

Acknowledgement

The authors express their thanks to the Agence Nationale de la Recherche (ANR) for financial support under contract ANR-16-CE08-0032-01 project MeTex and SATT Conectus project CoMet.

Appendix A. Supplementary data

Supplementary data to this article can be found online at https://doi.org/10.1016/j.matdes.2018.08.051.

References

[1] Y. Chaikin, O. Kedem, J. Raz, A. Vaskevich, I. Rubinstein, Anal. Chem. 85 (2013) 10022.
[2] G. Reina, S. Orlanducci, E. Tamburri, R. Matassa, M. Rossi, M.L. Terranova, Phys. Status Solidi C 13 (2016) 972.
[3] P. Rafighi, M. Tavahodi, B. Haghighi, Sensors Actuators B Chem. 232 (2016) 454.
[4] G. Yue, S. Su, N. Li, M. Shuai, X. Lai, D. Astruc, P. Zhao, Coord. Chem. Rev. 311 (2016) 75.
[5] M.-R. Zhang, X.-Q. Chen, G.-B. Pan, Sensors Actuators B Chem. 240 (2017) 142.
[6] M. Lin, H. Pei, F. Yang, C. Fan, X. Zuo, Adv. Mater. 25 (2013) 3490.
[7] H. Hau, D. Khanal, L. Rogers, N. Suchowerska, R. Kumar, S. Sridhar, D. McKenzie, W. Chrzanowski, Bioeng. Transl. Med. 1 (2016) 94.
[8] V. Gopinath, S. Priyadarshini, D. MubarakAli, M.F. Loke, N. Thajuddin, N.S. Alharbi, T. Yadavalli, M. Alagiri, J. Vadivelu, Arab. J. Chem. (2016)https://doi.org/10.1016/j.arabjc.2016.02.005.
[9] L. Zhang, Z.-S. Wang, J. Mater. Chem. C 4 (2016) 3614.
[10] A. Noschese, A. Buonerba, P. Canton, S. Milione, C. Capacchione, A. Grassi, J. Catal. 340 (2016) 30.
[11] R. Subair, B.P. Tripathi, P. Formanek, F. Simon, P. Uhlmann, M. Stamm, Chem. Eng. J. 295 (2016) 358.
[12] J. Kimling, M. Maier, B. Okenve, V. Kotaidis, H. Ballot, A. Plech, J. Phys. Chem. B 110 (2006) 15700.
[13] S.R.K. Perala, S. Kumar, Langmuir 29 (2013) 9863.
[14] N. Li, P. Zhao, D. Astruc, Angew. Chem. 53 (2014) 1756.
[15] H. Tyagi, A. Kushwaka, A. Kumar, M. Aslam, Nanoscale Res. Lett. 11 (2016) 362.
[16] L. Malassis, R. Dreyfus, R.J. Murphy, L.A. Hough, B. Donnio, C.B. Murray, RSC Adv. 6 (2016) 33092.
[17] C. Deraedt, L. Salmon, S. Gatard, R. Ciganda, R. Hernandez, J. Ruiz, D. Astruc, Chem. Commun. 50 (2014) 14194.
[18] a) N. Yao, W. Lin, X. Zhang, H. Gu, L. Zhang, J. Polym. Sci. A Polym. Chem. 54 (2016) 186;
b) M.R. Nabid, R. Sedghi, F. Eskandari, J. Nanomater. Mol. Nanotechnol. 2 (2013) 7.
[19] A. Jimenez-Ruiz, P. Perez-Tejeda, E. Grueso, P.M. Castillo, R. Prado-Gotor, Chem. Eur. J. 21 (2015) 9596.
[20] M. Iqbal, G. Usanase, K. Oulmi, F. Aberkane, T. Bendaikha, H. Fessi, N. Zine, G. Agusti, E.-S. Erracid, A. Elaissari, Mater. Res. Bull. 79 (2016) 97.
[21] T.K. Sau, A.L. Rogach, Adv. Mater. 22 (2010) 1781.
[22] J. Yan, Y. Pan, A.G. Cheetham, Y.-A. Lin, W. Wang, H. Cui, C.-J. Liu, Langmuir 29 (2013) 16051.
[23] M. Sangermano, A. Marchino, S. Perruchas, T. Gacoin, G. Rizza, Macromol. Mater. Eng. 293 (2008) 964.
[24] X. Wu, R. Kullock, E. Krauss, B. Hecht, Cryst. Res. Technol. 50 (2015) 595.
[25] P. Taranekar, C. Huang, T.M. Fulghum, A. Baba, G. Jiang, J.-Y. Park, R.C. Advincula, Adv. Funct. Mater. 18 (2008) 347.
[26] S. Ravaine, G.E. Fanucci, C.T. Seip, J.H. Adair, D.R. Talham, Langmuir 14 (1998) 708.
[27] S. Verma, B. Tirumala Rao, S. Rai, V. Ganesan, L.M. Kukreja, Appl. Surf. Sci. 258 (2012) 4898.
[28] M. Ghidelli, L. Mascaretti, B.R. Bricchi, A. Zapelli, V. Russo, C.S. Casari, A.L. Bassi, Appl. Surf. Sci. 434 (2018) 1064.
[29] S.-Q. Zhu, T. Zhang, X.-L. Guo, X. Liu, X.-Y. Zhang, Nanoscale Res. Lett. 7 (2012) 613.
[30] H. Li, J.J. Cooper-White, I. Kim, Soft Matter 9 (2013) 5270.
[31] A. Tyurin, G. De Filpo, D. Cupelli, F.P. Nicoletta, A. Mashin, G. Chidichimo, Express Polym. Lett. 4 (2010) 71.
[32] P. Alexandridis, M. Tsianou, Eur. Polym. J. 47 (2011) 569.
[33] T. Kim, S. Nam, S. Lim, H. Kim, Mol. Cryst. Liq. Cryst. 568 (2012) 170.
[34] H.E. Wael, K.A.-M. Yasser, A.A. Shabaka, M.H. Abd ElHameed, Spectrochim. Acta A Mol. Biomol. Spectrosc. 95 (2012) 341.
[35] S.S. Lamarre, S.A. Sarrazin, J. Proust, H. Yockell-Lelièvre, J. Plain, A.M. Ritcey, T. Maurer, J. Nanopart. Res. 15 (2013) 1656.
[36] L. Balan, M. Jin, J.P. Malval, H. Chaumeil, A. Defoin, L. Vidal, Macromolecules 41 (2008) 9359.

[37] J.-Y. Kim, D.-H. Shin, K.-J. Ihn, Macromol. Chem. Phys. 206 (2005) 794.
[38] a) L. Balan, V. Melinte, T. Buruiana, R. Schneider, L. Vidal, Nanotechnology 23 (2012), 415705. ;
b) L. Balan, J.-P. Malval, R. Schneider, D. Le Nouen, D.-J. Lougnot, Polymer 51 (2010) 1363;
c) S. Niu, R. Schneider, L. Vidal, L. Balan, Nanoscale 5 (2013) 6538;
d) S. Wolak, L. Vidal, J.-M. Becht, L. Michelin, L. Balan, Nanotechnology 27 (2016), 345601.
[39] H. Zhang, L. Wang, L. Song, G. Niu, H. Cao, G. Wang, H. Yang, S. Zhu, Appl. Polym. Sci. 121 (2011) 531.
[40] G. Kang, Y. Cao, H. Zhao, Q. Yuan, J. Membr. Sci. 318 (2008) 227.
[41] M. Bass, E.W. Van Stryland (Eds.), Handbook of Optics, second ed., Vol. 2, McGraw-Hill, ISBN: 0070479747, 1994.
[42] Al Usher, D.C. McPhail, J. Brugger, Geochim. Cosmochim. Acta 73 (2009) 3359.
[43] H. Kunkely, A. Vogler, Inorg. Chem. 31 (1992) 4539.
[44] H. Jung, H. Cha, D. Lee, S. Yoon, ACS Nano 9 (2015) 12292.
[45] B.S. Srinath, V. Ravishankar Rai, 3 Biotech. 5 (2015) 671.
[46] J. Qiu, W.D. Wei, J. Phys. Chem. C 118 (2014) 20735.
[47] M. Zaier, L. Vidal, S. Hajjar-Garreau, L. Balan, Sci. Report. 7 (2017) 12410.
[48] J. Polte, CrystEngComm 17 (2015) 6809.
[49] S. Porel, S. Singh, T.P. Radhakrishnan, Chem. Commun. 2387 (2005).
[50] S.-P. Chao, S. Jong, H.-N. Jo, S.-A. Lee, S. Bae, S.H. Lee, J. Hwang, H.-I. Joh, G. Wang, T.-W. Kim, J. Mater. Chem. C 4 (2016) 1511.
[51] M. Harada, S. Kizaki, Cryst. Growth Des. 16 (2016) 1200.
[52] T. Ung, L.M. Liz-Marzán, P. Mulvaney, J. Phys. Chem. B 105 (2001) 3441.
[53] K. Tanaka, K. Naka, E. Miyoshi, A. Narita, Y. Chujo, Polym. J. 47 (2015) 747.
[54] L. Guo, J.A. Jackman, H.-H. Yang, P. Chen, N.-J. Cho, D.H. Kim, Nano Today 10 (2015) 213.
[55] A. Hoffmann, Z. Lenkefi, Z. Szentirmay, J. Phys. Condens. Matter 10 (1998) 5503.
[56] S. Eustis, M.A. El-Sayed, Chem. Soc. Rev. 35 (2006) 209.
[57] J. Siegel, O. Lyntakov, V. Rybka, Z. Kolská, V. Švorčik, Nanoscale Res. Lett. 6 (2011) 96.
[58] A.V. Zayats, I.I. Smolyaninov, A.A. Maradudin, Phys. Rep. 408 (2005) 131.
[59] a) K. Leosson, J. Nanophotonics 6 (2012) 061801;
b) M. Kang, S.-G. Park, K.-H. Jeong, Sci. Rep. 5 (2015) 14790.